
ACCURATE GENERATION OF CHEMICAL REACTION TRANSITION STATES BY CONDITIONAL FLOW MATCHING

Ping Tuo

Bakar Institute of Digital Materials for the Planet
University of California, Berkeley
Berkeley, 94720, CA, United States
tuoping@berkeley.edu

Jiale Chen

Institute of Science and Technology Austria
Am Campus 1, 3400, Klosterneuburg, Austria

Ju Li

Department of Materials Science and Engineering
Massachusetts Institute of Technology
Cambridge, 02139, MA, United States
liju@mit.edu

July 15, 2025

ABSTRACT

Transition state (TS) structures define the critical geometries and energy barriers underlying chemical reactivity, yet their fleeting nature renders them experimentally elusive and drives the reliance on costly, high-throughput density functional theory (DFT) calculations. Here, we introduce TS-GEN, a conditional flow-matching generative model that maps samples from a simple Gaussian prior directly to transition-state saddle-point geometries in a single, deterministic pass. By embedding both reactant and product conformations as conditioning information, TS-GEN learns to transport latent noise to true TS structures via an optimal-transport path, effectively replacing the iterative optimization common in nudged-elastic band or string-method algorithms. TS-GEN delivers unprecedented accuracy, achieving a root-mean-square deviation of 0.004 Å (vs. 0.103 Å for prior state-of-the-art) and a mean barrier-height error of 1.019 kcal/mol (vs. 2.864 kcal/mol), while requiring only 0.06 s GPU time per inference. Over 87% of generated TSs meet chemical-accuracy criteria (< 1.58 kcal/mol error), substantially outpacing existing methods. TS-GEN also exhibits strong transferability to out-of-distribution reactions from a larger database. By uniting sub-angstrom precision, sub-second speed, and broad applicability, TS-GEN will be highly useful for high-throughput exploration of complex reaction networks, paving the way to the exploration of novel chemical reaction mechanisms.

1 Introduction

Transition state (TS) structures lie at the very heart of mechanistic chemistry. They define the precise bottleneck geometries and energy barriers that govern bond-breaking and bond-forming events, enabling the construction of detailed reaction networks for everything from combustion [1] and atmospheric processes [2] to enzymatic cascades [3] and materials degradation [4, 5]. Yet, because TSs reside at higher free energies than both reactants and products and endure for only femtoseconds, they remain experimentally elusive under ordinary conditions. To date, only a handful of “stroboscopic” techniques have succeeded in capturing TS signatures. For example, ultrafast millimetre-wave vibrational spectroscopy can infer barrier heights and structural features indirectly from rotational-vibrational fine structure [6], while femtosecond electron-diffraction experiments have yielded direct, picometer-scale snapshots of bond distances during photochemically triggered electrocyclic ring-opening [7]. Although powerful, these approaches are costly, technically demanding, and largely confined to small, gas-phase or matrix-isolated systems.

Consequently, the bulk of modern TS characterization is carried out *in silico*, where electronic-structure methods, most commonly density functional theory (DFT) [8] and coupled-cluster approaches such as CCSD(T) [9], supply the energies and gradients that underpin automated TS search algorithms. Traditional TS search techniques like the nudged elastic band (NEB) [10], string method [11], and dimer method [12] iteratively trace minimum energy pathways or directly converge on first-order saddle points by optimizing chains of images or perturbing along unstable modes. For a reasonably sized reaction network, however, thousands of TS structures need to be optimized, requiring millions of DFT single-point calculations [13]. The large number of chemical species involved in reaction networks thus drives an urgent need to reduce the computational cost of locating each TS.

Recently, machine learning (ML) has demonstrated promise for accelerating TS discovery. Early efforts include using ML potentials as surrogates for DFT within nudged-elastic band optimizations [14], recasting transition path sampling as a reinforcement-learning “shooting game” [15] or a stochastic optimal control problem [16], and viewing TS search as a 3D structure-generation task tackled by equivariant graph neural networks [17], generative-adversarial networks [18], gated-recurrent/transformer hybrids [19], denoising diffusion models [20, 21], or flow matching models [22]. Prior work such as React-OT [22] reformulates double-ended TS search via a flow matching framework that begins from a linear interpolation of reactant and product and deterministically transports to the TS by solving an ordinary differential equation (ODE). React-OT achieves state-of-the-art performance on generated structure similarity and barrier height, while reducing the inference evaluation time to a fraction of a second.

In this work, we developed TS-GEN, a conditional flow matching model that learns to map samples drawn from a simple Gaussian prior directly to transition state saddle point structures, embedding reactant and product conformations as conditions. By transporting latent noise to the true TS geometry in a single, deterministic pass, our method delivers an improvement in structural accuracy by 2 orders of magnitude (achieving a median root mean squared deviation (RMSD) of 0.0005 Å, and a median barrier height error of 0.251 kcal/mol) over prior state-of-the-art approaches, all while maintaining sub-second inference times per reaction. This unprecedented combination of precision and speed makes our flow-matching TS search ideally suited for high-throughput exploration of complex reaction networks, effectively replacing millions of costly DFT evaluations with one efficient generative step.

2 Results

2.1 TS-GEN: transition state generation by conditional flow matching

We build our generative model under the flow matching framework [23]. Given a continuous distribution of the coordinates of transition state structures $\mathbf{x}_1 \sim p_1$, we train a flow model $\mathbf{v}_\theta(\mathbf{x}, t)$ that transports a Gaussian prior distribution $\mathbf{x}_0 \sim p_0 \equiv \mathcal{N}(0, \mathbf{I})$ to the data p_1 . To do so, we define intermediate distributions $\mathbf{x}_t \sim p_t, t \in (0, 1)$ via $\mathbf{x}_t = t\mathbf{x}_1 + (1 - t)\mathbf{x}_0$, and train a neural network model \mathbf{v}_θ to approximate the flow field [23]

$$\mathbf{v}(\mathbf{x}_t, t) \equiv \mathbb{E}_{\mathbf{x}_0, \mathbf{x}_1}[\mathbf{x}_1 - \mathbf{x}_0] \quad (1)$$

which satisfies the transport equation $\partial p_t / \partial t + \nabla \cdot (p_t \mathbf{v}_t) = 0$.

Given a reactant and a product, our aim is to learn a generative model of transition states that minimizes the transition energy barrier. Therefore, we condition the generative model on the reactant and the product, as illustrated in Figure 1. The model learns to generate a distinct TS given each reactant-product pair.

2.2 Generating accurate TS structures in 0.06 s GPU time

We trained TS-GEN on Transition1x [24], a dataset that contains paired reactants, TSs and products calculated from climbing-image NEB [10] obtained with DFT (ω B97x/6-31G(d)) [25, 26]. Transition1x contains 11,961 reactions with product-reactant pairs sampled from the GDB-7 dataset [27]. Each reaction consists of up to seven heavy atoms including C, N, O, and 23 atoms in total. We use the same train-validation-test partitioning as reported with the database [24]. All datasets are stratified by molecular formula such that no two configurations that come from different data splits are constituted of the same atoms. Test and validation data each consist of 5% of the total data and are chosen such that configurations contain all heavy atoms (C, N, O). In TS-GEN, we use a GNN model with transformer-type message passing [28, 29] to predict the flow (see section 4.2 in the Methods for details of the model architecture).

TS-GEN achieves a mean RMSD of 0.004 Å between generated and true TS structures on the test reactions of Transition1x, improved upon the previous state-of-the-art (0.103 Å [22]) by 2 orders of magnitude. Similarly, TS-GEN reduces the mean error of barrier height estimation from the state-of-the-art value of 2.864 kcal/mol to 1.019 kcal/mol [22], highlighting the excellent accuracy of TS-GEN across all test reactions regardless of their level of complexity (Table 1). In chemical reactions, a difference of one order of magnitude in reaction rate is often used as the characterization

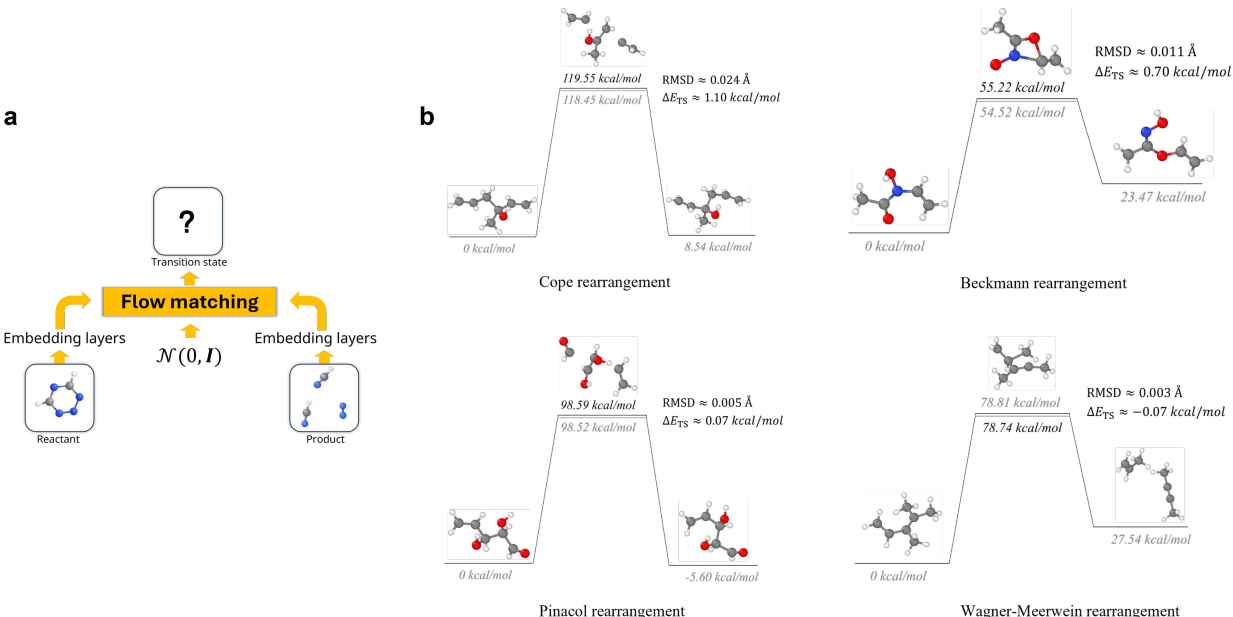


Figure 1: a, **Overview of the conditional flow matching framework for transition state generation.** We train a conditional flow matching model to follow the optimal transport mapping from a Gaussian prior to the transition state distribution. By embedding reactant and product structures as conditions, the model learns to generate a distinct TS tailored to each reaction. b, Example generations of named chemical reactions.

of chemical accuracy, which translates to 1.58 kcal/mol in barrier height error assuming a reaction temperature of 70 °C [30, 31]. With this definition, over 87% of TS from TS-GEN have high chemical accuracy, whereas the number is only 63% for state-of-the-art by React-OT and 71% for React-OT with pretraining [22].

Moreover, we find great transferability of TS-GEN on out-of-distribution reactions, which gives similar performance on a test set of 1,000 reactions randomly drawn from the bigger RGD1-CHNO database (with 176,992 reactions calculated with DFT (B3LYP-D3/TZVP)) [32]. Compared with Transition1x, RGD1-CHNO covers more diverse bond rearrangements during chemical reactions (see Figure 3). Even though the model was only trained on Transition1x data, the error on the RGD1-CHNO test set turned out even smaller (chemical accuracy 99.6%). We speculate that this is because the chemical reactions in RGD1-CHNO database are more realistic, thus conforming more to the underlying distribution of the TS, as the RGD1-CHNO database was built via a generic graph-based enumeration (see Supplementary Figure S3 for further details). Table 1 lists a performance comparison between more models.

TS-GEN learns an optimal path between the Gaussian prior and the TS. Thus, it necessarily only takes 2 ODE steps during inference. Both the RMSD and ΔE_{TS} reach roughly the same level using either 2 ODE steps, corresponding to an inference time of 0.06 s, or 50 ODE steps (see Table 1 for details).

3 Discussion

We developed TS-GEN, a conditional flow matching model for generating TSs, with the provided reactants and products as embedded conditions. TS-GEN exceeds the state-of-the-art accuracy by 2 orders of magnitude with an inference time within 0.06 s. The trained model shows great transferability to out-of-distribution data, and can be readily used for any neutral organic chemical space with C, N, O, H atoms. With the ability to generate accurate TSs, TS-GEN can be effectively used to explore reaction networks by integrating with a reaction network exploration package such as the Yet Another Reaction Program [34], as demonstrated by Duan et al [22]. In the future, it would be of great interest to generate more chemical reaction data with charged species and metals and train TS-GEN on more diverse chemistry to enable its application in more realistic chemical systems, such as those involving transition metal catalysts.

It is worth noting that the React-OT model by Duan et al [22] is also a flow matching model, yet its performance is not as good as TS-GEN. This can be attributed to many factors. One of them is that in React-OT, the linear interpolation of the reactant and product was used as prior distribution, instead of the Gaussian. Essentially, flow matching with

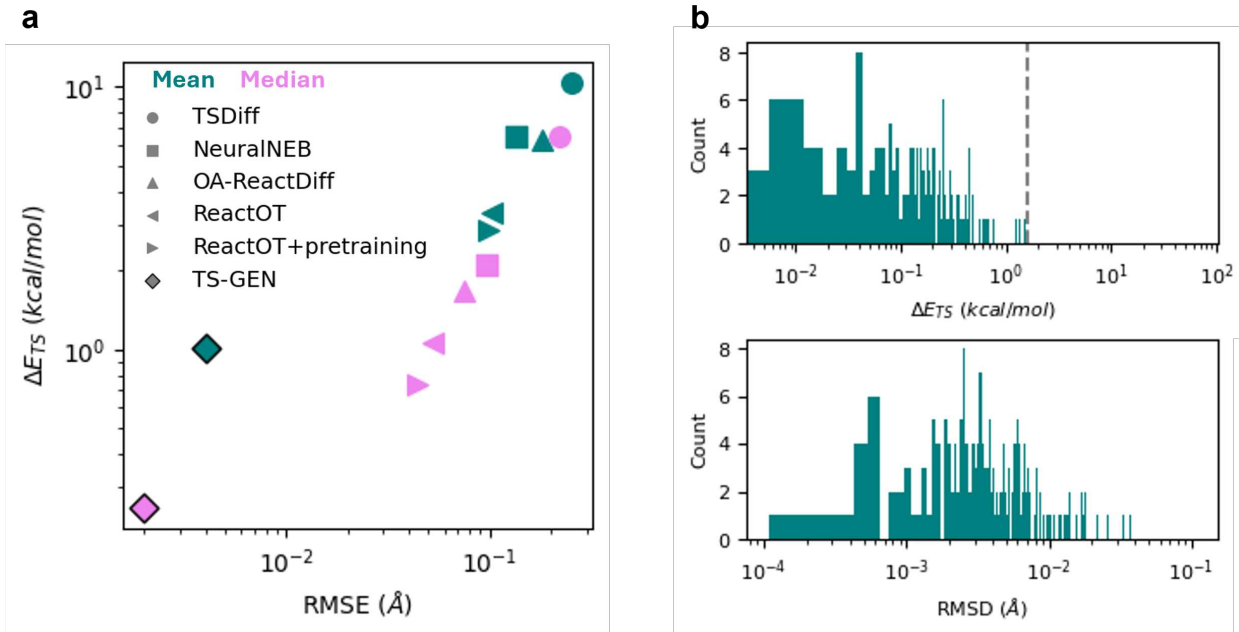


Figure 2: **a**, RMSD versus ΔE_{TS} for different TS generations approach, where the mean error is shown in teal and the median error is shown in violet. **b**, The ΔE_{TS} and RMSD of generated TS by TS-GEN for the test set. The threshold of chemical accuracy is indicated by a dashed line.

Table 1: Summary of statistics for RMSD, barrier height error, and inference time of TS structures. The statistics for models other than TS-GEN are from Duan et al [22]. For React-OT and TS-GEN, the inference time for 6 integration steps is shown, corresponding to where both the RMSD and barrier height error of React-OT converge. While for TS-GEN, the inference time for 2 integration steps is also shown in parentheses, where both the RMSD and barrier height error of TS-GEN already converge. Note that the inference time of NeuralNEB was evaluated on a central processing unit (CPU) [33].

Model	RMSD (Å)			ΔE_{TS} (kcal/mol)			Inference time (s)
	Mean	Median	Max	Mean	Median	%chem.acc.	
lrule TSDiff	0.253	0.221	-	10.369	6.428	10.9	-
NeuralNEB	0.136	0.096	-	6.510	2.114	42.6	33.00
OA-ReactDiff	0.180	0.075	-	6.256	1.681	49.7	6.80
OA-ReactDiff + recommender	0.130	0.058	-	4.453	1.617	48.7	272.00
React-OT	0.103	0.053	-	3.337	1.058	63.6	0.05
React-OT + pretraining	0.098	0.044	-	2.864	0.741	71.9	0.05
TS-GEN	0.004	0.002	0.163	1.019	0.251	87.8	0.18 (0.06)

optimal transport (OT) path learns a mapping from the prior to the target distribution. Using the same prior for all reactions ensures a more consistent OT path space. More importantly, in TS-GEN, we used the reactant and product states as embedded conditions, an approach also known as classifier-free guidance [35], to *intentionally induce selective mode collapse* towards the corresponding TS, thereby ensuring robust generation of the target TS (see Supplementary Figure S2 for an error distribution of multiple independently generated TS given the same reactant-product pair). On the other hand, in an earlier work by Duan et al [21], a diffusion model OA-ReactDiff was used to generate the TS structure starting from a Gaussian prior, whose performance was worse than React-OT. We speculate that this is due to the stochasticity of the diffusion process. To confirm this speculation, we have performed tests, where we vary the

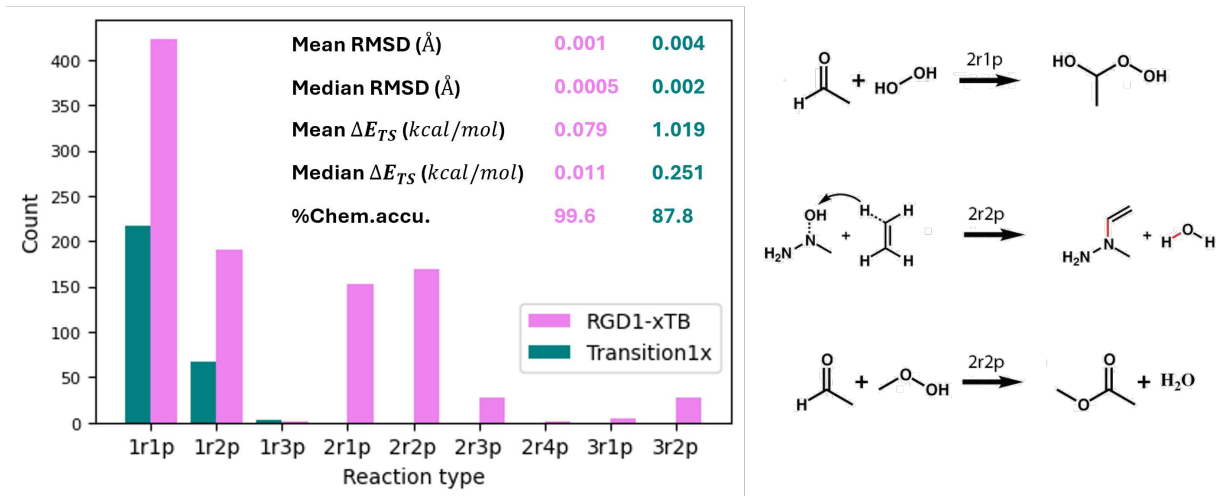


Figure 3: The distribution of reaction types in the test set sampled from Transition1x (teal) and RGD1-CHNO (violet). ArBp refers to a reaction that has A reactants and B products. Examples of reaction types that are presented exclusively in the test set of RGD1-CHNO are displayed. RMSD and ΔE_{TS} of the generated TS structure for Transition1x (teal) and RGD1-CHNO (violet), by the same TS-GEN model trained only by Transition1x data, are shown in text with corresponding color.

scheduling of the diffusion coefficient, and the diffusion model delivers the same level of accuracy as the flow matching model only when the diffusion coefficient is reduced to ≈ 0 near $t = 1$ (see Supplementary tests for details).

In this work, we only test our model on reactions with a single saddle point TS. But the model can be readily generalized to reactions with multiple transition steps. Although there are no reports on generating the TSs of multiple-step reactions due to the lack of a multistep reaction database, the problem can essentially be regarded as generating the molecular dynamics trajectory between two endpoint structures, where comprehensive toolboxes have already been implemented [36].

Although we demonstrate TS-GEN only on the TS search problem, there are many scenarios in biology, chemistry, and materials science where the flow matching generative model can be used to explore dynamic processes, including protein-ligand docking, molecule absorption on metal surfaces, and structural changes of materials in phase transitions. We anticipate that the TS-GEN model will be useful for applications in other domains of science.

4 Methods

4.1 Flow matching by optimal transport path

4.1.1 Preliminaries: continuous normalizing flows

Let \mathbb{R}^d denote the data space with points $\mathbf{x} = (x^1, \dots, x^d) \in \mathbb{R}^d$. Two important objects we use are: the probability density path $p : [0, 1] \times \mathbb{R}^d \rightarrow \mathbb{R}_{>0}$, which is a time-dependent density, and a time-dependent vector field $\mathbf{v} : [0, 1] \times \mathbb{R}^d \rightarrow \mathbb{R}^d$. A vector field \mathbf{v}_t generates a time-dependent diffeomorphism (a *flow*) $\phi : [0, 1] \times \mathbb{R}^d \rightarrow \mathbb{R}^d$ via the ODE

$$\frac{d}{dt}\phi_t(\mathbf{x}) = \mathbf{v}_t(\phi_t(\mathbf{x})), \quad (2)$$

$$\phi_0(\mathbf{x}) = \mathbf{x}. \quad (3)$$

Chen *et al.* [37] suggested modeling \mathbf{v}_t by a neural network $\mathbf{v}_t^{(\theta)}(\mathbf{x})$, where θ are learnable parameters, yielding a deep parametrization of the flow ϕ_t , called a continuous Normalizing Flow (CNF). A CNF pushes a simple base density p_0 (e.g. Gaussian noise) to a complex target p_1 via

$$p_t = [\phi_t]_* p_0, \quad (4)$$

where the push-forward operator is defined by the change-of-variables formula

$$[\phi_t]_* p_0(\mathbf{x}) = p_0(\phi_t^{-1}(\mathbf{x})) \det(\partial_{\mathbf{x}} \phi_t^{-1}(\mathbf{x})). \quad (5)$$

A vector field \mathbf{v}_t generates a density path p_t if its flow ϕ_t satisfies the above. Equivalently, one may verify the continuity equation

$$\partial_t p_t + \nabla \cdot (p_t \mathbf{v}_t) = 0. \quad (6)$$

4.1.2 Flow matching

Let \mathbf{x}_1 denote a random variable distributed according to some unknown data distribution $q(\mathbf{x}_1)$. Assume we only have access to data samples from $q(\mathbf{x}_1)$ but have no access to the density function itself. Furthermore, let p_0 be a simple distribution (e.g., the standard normal $p(\mathbf{x}) = \mathcal{N}(\mathbf{x}|0, I)$), and let p_1 be approximately equal in distribution to q . The Flow Matching objective is then designed to match a target probability path, which will allow us to flow from p_0 to p_1 .

A simple way to construct a target probability path is via a mixture of simpler conditional paths [23]. Given a data sample \mathbf{x}_1 , we denote by $p_t(\mathbf{x}|\mathbf{x}_1)$ a conditional probability path such that it satisfies $p_0(\mathbf{x}|\mathbf{x}_1) = p_0$ at $t = 0$, and we design $p_1(\mathbf{x}|\mathbf{x}_1)$ to be concentrated around \mathbf{x}_1 (e.g., $p_1(\mathbf{x}|\mathbf{x}_1) = \mathcal{N}(\mathbf{x}|\mathbf{x}_1, \sigma^2 I)$ for small $\sigma > 0$). Marginalizing over the unknown data distribution $q(\mathbf{x}_1)$ gives the marginal probability path [23]

$$p_t(\mathbf{x}) = \int p_t(\mathbf{x}|\mathbf{x}_1) q(\mathbf{x}_1) d\mathbf{x}_1, \quad (7)$$

which at $t = 1$ yields

$$p_1(\mathbf{x}) = \int p_1(\mathbf{x}|\mathbf{x}_1) q(\mathbf{x}_1) d\mathbf{x}_1 \approx q(\mathbf{x}). \quad (8)$$

One can also define a marginal vector field by “mixing” the conditional fields [23]:

$$u_t(\mathbf{x}) = \int u_t(\mathbf{x}|\mathbf{x}_1) \frac{p_t(\mathbf{x}|\mathbf{x}_1) q(\mathbf{x}_1)}{p_t(\mathbf{x})} d\mathbf{x}_1, \quad (9)$$

where each $u_t(\cdot|\mathbf{x}_1) : \mathbb{R}^d \rightarrow \mathbb{R}^d$ generates the conditional path $p_t(\cdot|\mathbf{x}_1)$. This aggregation yields the correct vector field for the marginal path $p_t(\mathbf{x})$.

4.1.3 Gaussian probability path

The Flow Matching objective works with any choice of probability path and vector field. We can construct $p_t(\mathbf{x}|\mathbf{x}_1)$ and $u_t(\mathbf{x}|\mathbf{x}_1)$ for a general family of Gaussian conditional paths [23]. Namely, we set

$$p_t(\mathbf{x}|\mathbf{x}_1) = \mathcal{N}(\mathbf{x}|\mu_t(\mathbf{x}_1), \sigma_t(\mathbf{x}_1)^2 I), \quad (10)$$

where $\mu : [0, 1] \times \mathbb{R}^d \rightarrow \mathbb{R}^d$ is a time-dependent mean and $\sigma : [0, 1] \times \mathbb{R} \rightarrow \mathbb{R}_{>0}$ a time-dependent standard deviation. We require $\mu_0(\mathbf{x}_1) = 0, \sigma_0(\mathbf{x}_1) = 1$ so that $p_0(\mathbf{x}|\mathbf{x}_1) = \mathcal{N}(\mathbf{x}|0, I)$, and $\mu_1(\mathbf{x}_1) = \mathbf{x}_1, \sigma_1(\mathbf{x}_1) = \sigma_{\min}$ with $\sigma_{\min} \ll 1$, so $p_1(\mathbf{x}|\mathbf{x}_1)$ concentrates at \mathbf{x}_1 .

Among the infinitely many vector fields generating this path (e.g., differing by divergence-free terms), Lipman *et al.* proposed to choose the simplest affine flow conditioned on \mathbf{x}_1 [23]:

$$\psi_t(\mathbf{x}) = \sigma_t(\mathbf{x}_1) \mathbf{x} + \mu_t(\mathbf{x}_1), \quad (11)$$

which pushes the standard normal $p_0(\mathbf{x}|\mathbf{x}_1) = \mathcal{N}(\mathbf{x}|0, I)$ to $p_t(\mathbf{x}|\mathbf{x}_1)$ via

$$[\psi_t]_* p_0(\mathbf{x}) = p_t(\mathbf{x}|\mathbf{x}_1). \quad (12)$$

The associated vector field then follows from differentiating the flow:

$$\frac{d}{dt} \psi_t(\mathbf{x}) = u_t(\psi_t(\mathbf{x})|\mathbf{x}_1). \quad (13)$$

Reparameterizing $\mathbf{x} = \psi_t(\mathbf{x}_0)$ gives the CFM loss:

$$\mathcal{L}_{\text{CFM}}(\theta) = \mathbb{E}_{t \sim \mathcal{U}[0,1], q(\mathbf{x}_1), p(\mathbf{x}_0)} \left\| \mathbf{v}_t^\theta(\psi_t(\mathbf{x}_0)) - \frac{d}{dt} \psi_t(\mathbf{x}_0) \right\|^2, \quad (14)$$

where θ are learnable parameters of a neural network model. Since ψ_t is an invertible affine map, one can compute u_t in closed form from $\frac{d}{dt}\psi_t$.

Let $p_t(\mathbf{x}|\mathbf{x}_1)$ be a Gaussian probability path as in equation (10), and let ψ_t be its corresponding flow map as in equation (11). Then the unique vector field that defines ψ_t has the form

$$u_t(\mathbf{x}|\mathbf{x}_1) = \frac{\sigma'_t(\mathbf{x}_1)}{\sigma_t(\mathbf{x}_1)}(\mathbf{x} - \mu_t(\mathbf{x}_1)) + \mu'_t(\mathbf{x}_1). \quad (15)$$

Consequently, $u_t(\mathbf{x}|\mathbf{x}_1)$ generates the Gaussian path $p_t(\mathbf{x}|\mathbf{x}_1)$.

4.1.4 Optimal transport path

A natural choice for probability paths is to define the mean and the std to simply change linearly in time:

$$\mu_t(\mathbf{x}_1) = t\mathbf{x}_1, \quad \sigma_t(\mathbf{x}_1) = 1 - (1 - \sigma_{\min})t. \quad (16)$$

Then this path is generated by the vector field [23]

$$u_t(\mathbf{x}|\mathbf{x}_1) = \frac{\mathbf{x}_1 - (1 - \sigma_{\min})\mathbf{x}}{1 - (1 - \sigma_{\min})t}. \quad (17)$$

The conditional flow that corresponds to $u_t(\mathbf{x}|\mathbf{x}_1)$ is

$$u_t(\mathbf{x}) = \mathbf{x}_1 - (1 - \sigma_{\min})\mathbf{x}_0. \quad (18)$$

Allowing the mean and std to change linearly not only leads to simple and intuitive paths, but it is actually also optimal in the following sense. The conditional flow $p_t(\mathbf{x}|\mathbf{x}_1)$ is in fact the Optimal Transport (OT) displacement map between the two Gaussians $p_0(\mathbf{x}|\mathbf{x}_1) = \mathcal{N}(\mathbf{x}|0, I)$ and $p_1(\mathbf{x}|\mathbf{x}_1)$.

In order to learn a parametrized $\mathbf{v}^{(\theta)} = \partial_t \mathbf{x}(t)$, we minimize the regression based objective [38]

$$L[\mathbf{v}^{(\theta)}] = \mathbb{E}_{\mathbf{x}_0, \mathbf{x}_1, t} \left[\frac{1}{2} |\mathbf{v}^{(\theta)}(t, \mathbf{x})|^2 - (u_t(\mathbf{x}|\mathbf{x}_1) \cdot \mathbf{v}^{(\theta)}(t, \mathbf{x})) \right]. \quad (19)$$

Note that the objective in Eq. 19 can also be written as

$$L[\mathbf{v}^{(\theta)}] = \mathbb{E}_{\mathbf{x}_0, t} \int_{\mathbb{R}^d} \left(\frac{1}{2} |\mathbf{v}^{(\theta)}(t, \mathbf{x}|\mathbf{x}_1)|^2 - u_t(\mathbf{x}|\mathbf{x}_1) \cdot \mathbf{v}^{(\theta)}(t, \mathbf{x}|\mathbf{x}_1) \right) p(\mathbf{x}_1) d\mathbf{x}_1. \quad (20)$$

Therefore, we can "bake in" the distribution of the TS structures by rewriting the loss in terms of the barrier height with $p(\mathbf{x}_1) = e^{-\beta E_{\text{TS}}(\mathbf{x}_1)}$.

4.2 Flow model architecture

The GNN flow model consists of three components: an Encoder, a Processor (for message passing), and a Decoder [28]. The atomic graph is denoted as (V, E) , where V is a set of node features $\{\mathbf{h}_i\}$ for node atom i , and E is a set of edge/bond features $\{\mathbf{e}_{ij}\}$ from node i to node j . The set of edges E is determined by a cutoff distance $r_c = 12 \text{ \AA}$, within which a pair of nodes form an edge connection.

In the Encoder stage, the node features are computed as an embedding of the one-hot encoded atom type z :

$$\mathbf{h}_i \leftarrow M_H(\mathbf{z}_i), \quad (21)$$

where M_H is a linear layer. The edge feature \mathbf{e}_{ij} is the concatenation of the edge vectors $\mathbf{r}_{ij} = \mathbf{r}_j - \mathbf{r}_i$ and the corresponding edge lengths $|\mathbf{r}_{ij}|$, followed by a multilayer perceptron (MLP) M_E :

$$\mathbf{e}_{ij} \leftarrow M_E(\mathbf{r}_{ij} \oplus |\mathbf{r}_{ij}|), \quad (22)$$

where \oplus designates concatenation of features. M_E consists of two dense linear layers, with SiLU activation function. Each node's scalar feature was computed by a convolution:

$$\mathbf{h}_i \leftarrow \phi_h(\mathbf{h}_i \oplus \phi_s(\sum_j \mathbf{h}_j \oplus \mathbf{e}_{ij})), \quad (23)$$

where ϕ_h and ϕ_s are MLPs. For flow model, each node’s vector features are computed as a weighted sum of its neighboring features

$$\mathbf{e}_i = \sum_j \phi_v(\mathbf{h}_i \oplus \mathbf{h}_j \oplus \mathbf{e}_{ij}) \mathbf{r}_{ij}, \quad (24)$$

where ϕ_v is a MLP. ϕ_h , ϕ_s , and ϕ_v consist of two dense linear layers, with SiLU activation function.

The ODE time t was embedded by a MLP and added to the node features \mathbf{h}_i . To condition on the reactant and product (RP), we embed the RP coordinates by a linear layer, and add the conditioning representations also to the node features \mathbf{h}_i .

Note that the atomic graphs obtained here are not equivariant. While one can ordinarily recover rotational equivariance through data augmentation (e.g. randomly rotating all coordinates at training time), doing so would disrupt the fixed relative orientation between the RP and the TS. In TS generation, that inter-state angle is a meaningful degree of freedom that must be preserved. Consequently, we neither impose equivariance in the RP conditioning nor enforce it on the generated graph, ensuring the reactant, TS, and product geometries remain correctly aligned.

We used the equivariant transformer [29] as the Processor (refer to the original paper for further details).

The Decoder is a simple linear layer M_O that maps the node features into the prediction output:

$$\hat{y}_i \leftarrow M_O(\mathbf{h}_i). \quad (25)$$

For the score model, the Decoder maps the edge features into the prediction vector:

$$\mathbf{v}_i \leftarrow M_O^v(\mathbf{e}_i). \quad (26)$$

M_O and M_O^v are both linear layers.

Model parameters are listed in the Supplementary Table S1.

4.3 Details for model training and evaluation

Model training We used a learning rate of 0.0001 and dropped it to 0.00001 for fine-tuning when the loss is roughly converged. The batch size was set to 1, and the model was trained for 200 epochs.

Evaluation The energies of the generated TS structures were calculated using MACE-OFF foundational model [39]. The energies of the corresponding true TS structures are evaluated using the same model for error evaluation.

5 Code availability

The code base for TS-GEN is available as an open-source repository for contiguous development, at <https://github.com/tuoping/TS-GEN>.

References

- [1] Tianfeng Lu and Chung K Law. Toward accommodating realistic fuel chemistry in large-scale computations. *Progress in Energy and Combustion Science*, 35(2):192–215, 2009.
- [2] Abdelwahid Mellouki, TJ Wallington, and J Chen. Atmospheric chemistry of oxygenated volatile organic compounds: impacts on air quality and climate. *Chemical reviews*, 115(10):3984–4014, 2015.
- [3] Souvik Ghosh, Mathieu G Baltussen, Nikita M Ivanov, Rianne Haije, Miglè Jakšaitė, Tao Zhou, and Wilhelm TS Huck. Exploring emergent properties in enzymatic reaction networks: design and control of dynamic functional systems. *Chemical Reviews*, 124(5):2553–2582, 2024.
- [4] Celine V Aarsen, Anna Liguori, Rebecca Mattsson, Mika H Sipponen, and Minna Hakkarainen. Designed to degrade: tailoring polyesters for circularity. *Chemical Reviews*, 124(13):8473–8515, 2024.
- [5] Haiyang Yu, Andrés Díaz, Xu Lu, Binhun Sun, Yu Ding, Motomichi Koyama, Jianying He, Xiao Zhou, Abdelali Oudriss, Xavier Feaugas, et al. Hydrogen embrittlement as a conspicuous material challenge— comprehensive review and future directions. *Chemical Reviews*, 124(10):6271–6392, 2024.
- [6] Kirill Prozument, Joshua H Baraban, P Bryan Changala, G Barratt Park, Rachel G Shaver, John S Muentert, Stephen J Klippenstein, Vladimir Y Chernyak, and Robert W Field. Photodissociation transition states characterized by chirped pulse millimeter wave spectroscopy. *Proceedings of the National Academy of Sciences*, 117(1):146–151, 2020.

- [7] Yusong Liu, David M Sanchez, Matthew R Ware, Elio G Champenois, Jie Yang, J Pedro F Nunes, Andrew Attar, Martin Centurion, James P Cryan, R Forbes, et al. Rehybridization dynamics into the pericyclic minimum of an electrocyclic reaction imaged in real-time. *Nature Communications*, 14(1):2795, 2023.
- [8] Narbe Mardirossian and Martin Head-Gordon. Thirty years of density functional theory in computational chemistry: an overview and extensive assessment of 200 density functionals. *Molecular physics*, 115(19):2315–2372, 2017.
- [9] Rodney J Bartlett and Monika Musiał. Coupled-cluster theory in quantum chemistry. *Reviews of Modern Physics*, 79(1):291–352, 2007.
- [10] Graeme Henkelman, Blas P Uberuaga, and Hannes Jónsson. A climbing image nudged elastic band method for finding saddle points and minimum energy paths. *The Journal of chemical physics*, 113(22):9901–9904, 2000.
- [11] E Weinan, Weiqing Ren, and Eric Vanden-Eijnden. String method for the study of rare events. *Physical Review B*, 66(5):052301, 2002.
- [12] Graeme Henkelman and Hannes Jónsson. A dimer method for finding saddle points on high dimensional potential surfaces using only first derivatives. *The Journal of chemical physics*, 111(15):7010–7022, 1999.
- [13] Johannes T Margraf, Hyunwook Jung, Christoph Scheurer, and Karsten Reuter. Exploring catalytic reaction networks with machine learning. *Nature Catalysis*, 6(2):112–121, 2023.
- [14] Shuhao Zhang, Małgorzata Z Makoś, Ryan B Jadrich, Elfi Kraka, Kipton Barros, Benjamin T Nebgen, Sergei Tretiak, Olexandr Isayev, Nicholas Lubbers, Richard A Messerly, et al. Exploring the frontiers of condensed-phase chemistry with a general reactive machine learning potential. *Nature Chemistry*, 16(5):727–734, 2024.
- [15] Jun Zhang, Yao-Kun Lei, Zhen Zhang, Xu Han, Maodong Li, Lijiang Yang, Yi Isaac Yang, and Yi Qin Gao. Deep reinforcement learning of transition states. *Physical Chemistry Chemical Physics*, 23(11):6888–6895, 2021.
- [16] Lars Holdijk, Yuanqi Du, Ferry Hooft, Priyank Jaini, Berend Ensing, and Max Welling. Stochastic optimal control for collective variable free sampling of molecular transition paths. *Advances in Neural Information Processing Systems*, 36:79540–79556, 2023.
- [17] Puck van Gerwen, Ksenia R Briling, Charlotte Bunne, Vignesh Ram Somnath, Ruben Laplaza, Andreas Krause, and Clemence Corminboeuf. 3dreact: Geometric deep learning for chemical reactions. *Journal of chemical information and modeling*, 64(15):5771–5785, 2024.
- [18] Małgorzata Z Makoś, Niraj Verma, Eric C Larson, Marek Freindorf, and Elfi Kraka. Generative adversarial networks for transition state geometry prediction. *The Journal of Chemical Physics*, 155(2), 2021.
- [19] Sunghwan Choi. Prediction of transition state structures of gas-phase chemical reactions via machine learning. *Nature Communications*, 14(1):1168, 2023.
- [20] Seonghwan Kim, Jeheon Woo, and Woo Youn Kim. Diffusion-based generative ai for exploring transition states from 2d molecular graphs. *Nature Communications*, 15(1):341, 2024.
- [21] Chenru Duan, Yuanqi Du, Haojun Jia, and Heather J Kulik. Accurate transition state generation with an object-aware equivariant elementary reaction diffusion model. *Nature computational science*, 3(12):1045–1055, 2023.
- [22] Chenru Duan, Guan-Horng Liu, Yuanqi Du, Tianrong Chen, Qiyan Zhao, Haojun Jia, Carla P Gomes, Evangelos A Theodorou, and Heather J Kulik. Optimal transport for generating transition states in chemical reactions. *Nature Machine Intelligence*, 7(4):615–626, 2025.
- [23] Yaron Lipman, Ricky TQ Chen, Heli Ben-Hamu, Maximilian Nickel, and Matt Le. Flow matching for generative modeling. *arXiv preprint arXiv:2210.02747*, 2022.
- [24] Mathias Schreiner, Arghya Bhowmik, Tejs Vegge, Jonas Busk, and Ole Winther. Transition1x-a dataset for building generalizable reactive machine learning potentials. *Scientific Data*, 9(1):779, 2022.
- [25] Jeng-Da Chai and Martin Head-Gordon. Systematic optimization of long-range corrected hybrid density functionals. *The Journal of chemical physics*, 128(8), 2008.
- [26] RHWJ Ditchfield, Warren J Hehre, and John A Pople. Self-consistent molecular-orbital methods. ix. an extended gaussian-type basis for molecular-orbital studies of organic molecules. *The Journal of Chemical Physics*, 54(2):724–728, 1971.
- [27] Lars Ruddigkeit, Ruud Van Deursen, Lorenz C Blum, and Jean-Louis Reymond. Enumeration of 166 billion organic small molecules in the chemical universe database gdb-17. *Journal of chemical information and modeling*, 52(11):2864–2875, 2012.
- [28] Hyuna Kwon, Tim Hsu, Wenyu Sun, Wonseok Jeong, Fikret Aydin, James Chapman, Xiao Chen, Vincenzo Lordi, Matthew R Carbone, Deyu Lu, et al. Spectroscopy-guided discovery of three-dimensional structures of disordered materials with diffusion models. *Machine Learning: Science and Technology*, 5(4):045037, 2024.

- [29] Wenbing Huang, Rui Jiao, Xiangzhe Kong, Li Zhang, Ziyang Yu, Fangyuan Ren, Wenjuan Tan, and Yang Liu. An equivariant pretrained transformer for unified 3d molecular representation learning. 2025.
- [30] Haohao Fu, Yan Zhou, Xiang Jing, Xueguang Shao, and Wensheng Cai. Meta-analysis reveals that absolute binding free-energy calculations approach chemical accuracy. *Journal of Medicinal Chemistry*, 65(19):12970–12978, 2022.
- [31] Éric Brémond, Hanwei Li, Ángel José Pérez-Jiménez, Juan Carlos Sancho-García, and Carlo Adamo. Tackling an accurate description of molecular reactivity with double-hybrid density functionals. *The Journal of Chemical Physics*, 156(16), 2022.
- [32] Qiyuan Zhao, Sai Mahit Vaddadi, Michael Woulfe, Lawal A Ogunfowora, Sanjay S Garimella, Olexandr Isayev, and Brett M Savoie. Comprehensive exploration of graphically defined reaction spaces. *Scientific Data*, 10(1):145, 2023.
- [33] Mathias Schreiner, Arghya Bhowmik, Tejs Vegge, Peter Bjørn Jørgensen, and Ole Winther. Neuralneb—neural networks can find reaction paths fast. *Machine Learning: Science and Technology*, 3(4):045022, 2022.
- [34] Qiyuan Zhao and Brett M Savoie. Simultaneously improving reaction coverage and computational cost in automated reaction prediction tasks. *Nature Computational Science*, 1(7):479–490, 2021.
- [35] Jonathan Ho and Tim Salimans. Classifier-free diffusion guidance. *arXiv preprint arXiv:2207.12598*, 2022.
- [36] Bowen Jing, Hannes Stärk, Tommi Jaakkola, and Bonnie Berger. Generative modeling of molecular dynamics trajectories. *arXiv preprint arXiv:2409.17808*, 2024.
- [37] Ricky TQ Chen, Yulia Rubanova, Jesse Bettencourt, and David K Duvenaud. Neural ordinary differential equations. *Advances in neural information processing systems*, 31, 2018.
- [38] Michael S Albergo, Nicholas M Boffi, and Eric Vanden-Eijnden. Stochastic interpolants: A unifying framework for flows and diffusions. *arXiv preprint arXiv:2303.08797*, 2023.
- [39] Dávid Péter Kovács, J Harry Moore, Nicholas J Browning, Ilyes Batatia, Joshua T Horton, Yixuan Pu, Venkat Kapil, William C Witt, IB Magdău, Daniel J Cole, et al. Mace-off: Transferable short range machine learning force fields for organic molecules. *arXiv preprint arXiv:2312.15211*, 2025.

SUPPLEMENTARY MATERIAL OF "ACCURATE GENERATION OF CHEMICAL REACTION TRANSITION STATES BY CONDITIONAL FLOW MATCHING"

Ping Tuo

Bakar Institute of Digital Materials for the Planet
University of California, Berkeley
Berkeley, 94720, CA, United States
tuoping@berkeley.edu

Jiale Chen

Institute of Science and Technology Austria
Am Campus 1, 3400, Klosterneuburg, Austria

Ju Li

Department of Materials Science and Engineering
Massachusetts Institute of Technology
Cambridge, 02139, MA, United States
liju@mit.edu

July 15, 2025

Contents

I	Supplementary tests	1
----------	----------------------------	----------

List of Tables

S1	Model parameters.	2
----	---------------------------	---

List of Figures

S1	SDE vs. ODE	2
S2	Robustness test	3
S3	Outlier reactions	3

I Supplementary tests

To quantify the difference between the ODE-based flow matching and the SDE-based diffusion, we adopt the Schrödinger bridge technique [1], where we train a separate score model $s^{(\theta)}(t, \mathbf{x}(t)) = \nabla_{\mathbf{x}} \log p(t)$. For processes where $p(t)$ are Gaussian, the score is calculated by

$$s^{(\theta)}(t, \mathbf{x}(t)) = \nabla_{\mathbf{x}} \log p(t) = \frac{t\mathbf{x}_1 + (1-t)\mathbf{x}_0 - \mathbf{x}}{\sigma^2 t(1-t)}, \quad (\text{S1})$$

where σ is the variance of the Gaussian distribution. Then we can approximate the SDE with a flow (drift) model and a score model as:

$$\frac{d\mathbf{x}_t}{dt} = -\mathbf{v}^{(\theta)}(t, \mathbf{x}_t) + \frac{g(t)^2}{2} \mathbf{s}^{(\theta)}(t, \mathbf{x}_t) + g(t) \frac{dw_t}{dt}. \quad (\text{S2})$$

We tested SDE with three different scheduling of the diffusion coefficient $\frac{g(t)^2}{2}$ on the generation of selected atoms in a *CrCoNi* lattice, and benchmarked them against ODE (Figure S1). Only the SDE starting with an increase in diffusion coefficient and then decreases in diffusion coefficient (towards 0 at $t = 1$) manages to deliver a performance similar to the ODE. This indicates that two factors are necessary for optimal performance of diffusion: the first is a long enough diffusion time plus a large enough diffusion coefficient, which can be substituted with a predictor-corrector sampling strategy [2]; the second is a near-zero diffusion coefficient near $t = 1$.

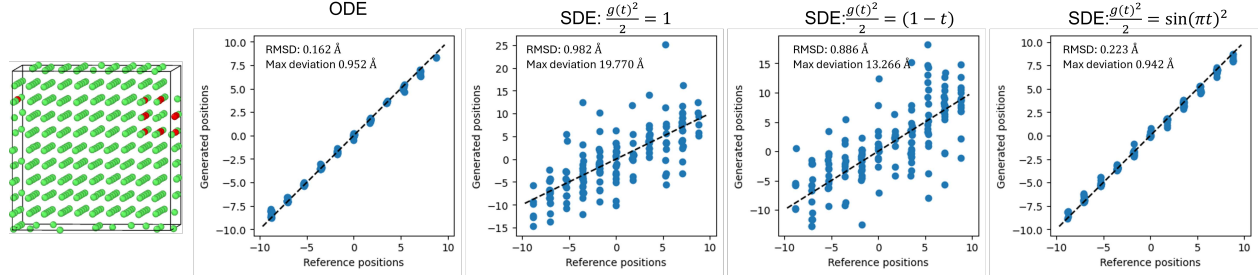


Figure S1: Error of the generated coordinates by ODE, SDE with constant diffusion coefficient, SDE with linearly decreasing diffusion coefficient, and SDE with increasing-then-decreasing diffusion coefficient. The target was selected atoms in a *CrCoNi*-fcc lattice (first nearest neighbors of vacancies, shown in red). SDE with increasing-then-decreasing diffusion coefficient delivers an accuracy similar to ODE.

Table S1: Model parameters.

Dim of the one hot atom type vector		5
Encoder	M_H	5×384
	M_E	$4 \times 64 \times 64$
	ϕ_s	$(384 + 384 + 64) \times 64 \times 384$
	ϕ_h	$(384 + 384) \times 64 \times 384$
	ϕ_v	$(384 + 384 + 64) \times 64 \times 384$
Processor	num of transformer layers	5
	num of heads	4
	head size	64
	hidden dim	64
Decoder	M_O^v	384×1
r_c		12 \AA

References

- [1] Alexander Tong, Nikolay Malkin, Kilian Fatras, Lazar Atanackovic, Yanlei Zhang, Guillaume Huguette, Guy Wolf, and Yoshua Bengio. Simulation-free schrödinger bridges via score and flow matching. *arXiv preprint arXiv:2307.03672*, 2023.
- [2] Yang Song, Jascha Sohl-Dickstein, Diederik P Kingma, Abhishek Kumar, Stefano Ermon, and Ben Poole. Score-based generative modeling through stochastic differential equations. *arXiv preprint arXiv:2011.13456*, 2020.

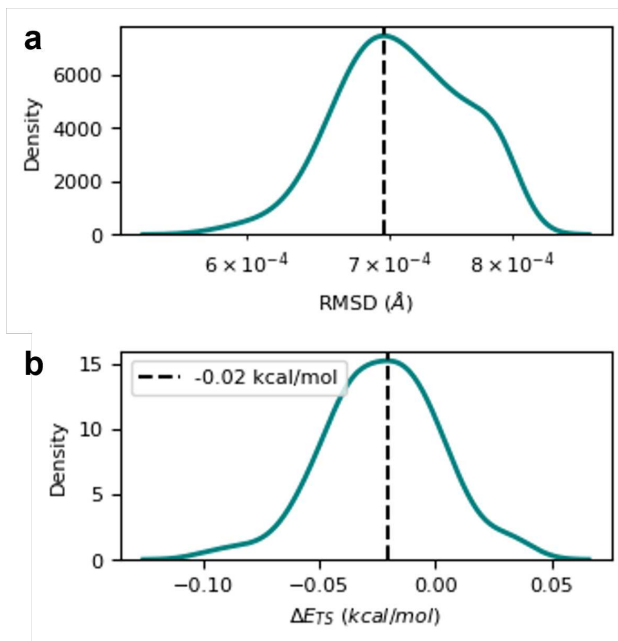


Figure S2: The distribution of the (a) RMSD, and (b) ΔE_{TS} , of 100 independently generated TS given the same reactant-product pair.

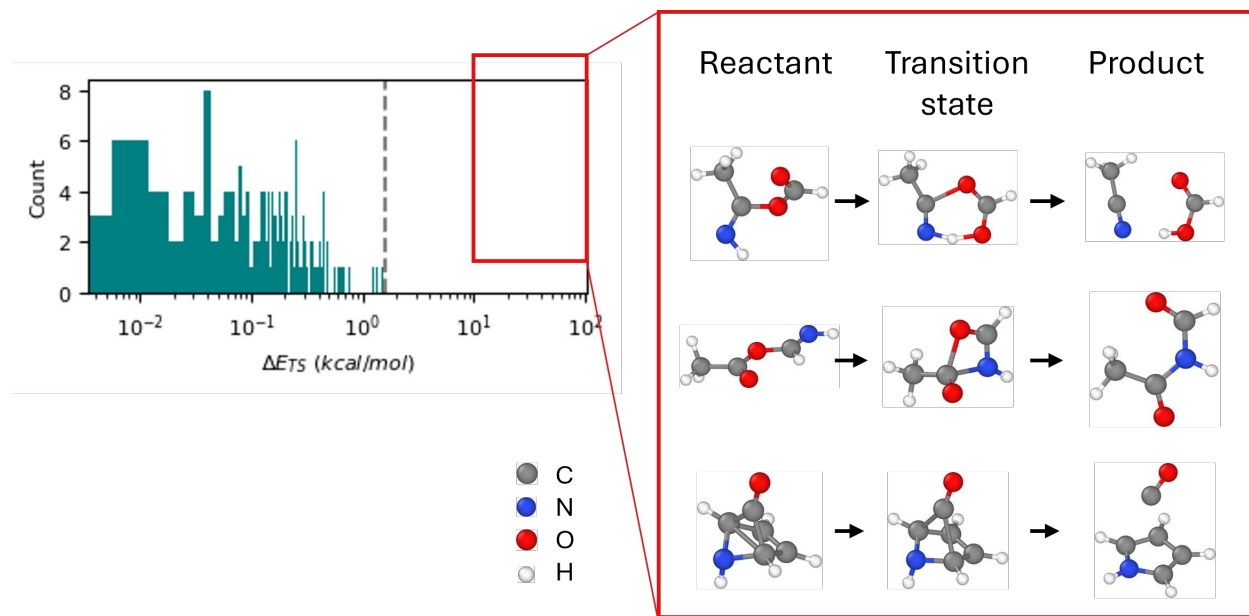


Figure S3: We found three outlier reactions from the Transition1x test set, whose RMSD are 0.066 \AA , 0.063 \AA , and 0.107 \AA (from up to bottom), and ΔE_{TS} are 17.854 kcal/mol , 26.310 kcal/mol , and 63.890 kcal/mol (from up to bottom) respectively. All of them turned out to be unphysical. In the first reaction from the top, the $C - O - C$ bond angle in the reactant was 118.14° , out of the expected range of $109^\circ - 112^\circ$. In addition, at equilibrium, the reactant is supposed to fold in, forming a $N - H \cdots O = C$ hydrogen bond, while the configuration shown here is actually a non-equilibrium state. Similarly, in the second reaction, the $C - O - C$ bond angle in the reactant was 120.96° , way out of the expected range. In the third reaction, the coordination of C atoms in the reactant are obviously violating the octet rule.